Scanning Near-Field and Confocal Raman Microscopic Investigation of P3HT−PCBM Systems for Solar Cell Applications

E. Klimov,[†] W. Li,[†,§] X. Yang,[†,‡] G. G. Hoffmann[†,⊥] and J. Loos*[,†,‡]

Laboratory of Materials and Interface Chemistry and Dutch Polymer Institute, Eindhoven University of Technology, Eindhoven, The Netherlands; Department of Macromolecular Science, Fudan University, Shanghai, China; and Laboratory of Molecular and Polymer Spectroscopy, University of Duisburg-Essen, Essen, Germany

Received December 4, 2005; Revised Manuscript Received April 19, 2006

ABSTRACT: The morphological evolution of thin composite films based on poly(3-hexylthiophene) (P3HT) and [6,6]-phenyl C_{61} butyric acid methyl ester (PCBM) upon annealing has been studied by means of transmission electron microscopy (TEM), scanning near-field optical microscopy (SNOM), and confocal Raman microscopy. This system currently is the most promising candidate for high-performance polymer solar cells. TEM bright field and SNOM topography measurements show that segregation and large-scale crystallization of PCBM take place upon thermal annealing. Additional SNOM optical absorbance measurements using laser irradiation sources with two different wavelengths in the visible light range and Raman microscopy are able to detect the component distribution within the thin composite film, which in detail demonstrates high diffusive mobility of PCBM upon annealing.

Introduction

Polymer solar cells[1] are a new type of photovoltaic conversion devices with high potential applications in the future energy market since their unique advantages in potential low production costs because of roll-to-roll production, their flexibility, and light weight. In contrast to many inorganic semiconductors, in which photon absorption directly produces free electrons and holes,[2] optical absorption in organic molecular and polymer semiconductors mainly creates electron−hole pairs (excitons) that are bound at room temperature.[3] In bulk-heterojunction[4,5] photovoltaic cells the creation of free electrons and holes is accomplished by the spontaneous dissociation of the excitons at the donor/acceptor interface.[6] Subsequent transport and collection of the photoinduced charges at the appropriate electrodes then provides the photovoltaic effect. Morphology manipulation of the photoactive layer is thus a key point to improve the device performance of polymer solar cells.[7−11]

In terms of efficiency and stability, one of the most promising polymer solar cells developed to date is based on the combination of regioregular poly(3-hexylthiophene) (P3HT) as donor and [6,6]-phenyl C_{61} butyric acid methyl ester (PCBM) as acceptor (Scheme 1).[12,13] External quantum efficiencies above 75% and power conversion efficiencies of up to 3.85% have been reported recently for these P3HT:PCBM devices.[14] The high efficiency of these devices can be related to the intrinsic properties of the two components. Regioregular P3HT self-organizes into a microcrystalline structure,[15] and because of efficient interchain transport of charge carriers, the (hole) mobility in P3HT is high (up to $\sim$0.1 cm^2 V^{-1} s^{-1}).[16−18] Moreover, in thin films interchain interactions cause a red shift of the optical absorption of P3HT, which provides an improved overlap with the solar emission. The second component, PCBM, is a C_{60} fullerene derivative with an electron mobility of 2×10^{-3} cm^2 V^{-1} s^{-1}.[19] Compared to C_{60}, the solubility of PCBM in organic solvents is greatly improved, which allows the utilization of film deposition techniques requiring highly concentrated solution.

Scheme 1. Donor−Acceptor Pair for Polymer Solar Cells Containing Poly(3-hexylthiophene) P3HT (left) and [6,6]-Phenyl C61-Butyric Acid Methyl Ester PCBM (right)

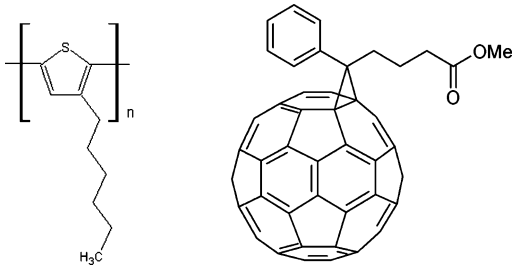

Interestingly, the efficiency of solar cells based on P3HT and fullerenes was shown to depend strongly on the processing conditions and to improve particularly by a post-thermal annealing step.[13,20−24] During annealing, crystal growth and crystal perfection of both components occur, which increases charge transport capability. However, continuous annealing forces aggregation of both P3HT and PCBM, particularly the PCBM component, resulting in large-scale phase separation in the composite film. This goes hand in hand with decreasing performance of the device. Thus, accurate control of the annealing conditions is essential to gain high-performance devices, and procedures to monitor phase segregation upon annealing are required.

In this study, we introduce an approach to achieve detailed information on the morphology evolution and local composition of P3HT/PCBM composite films upon annealing by means of scanning near-field optical microscopy (SNOM) and Raman spectroscopy. Combination of both techniques provides a close look on the phase segregation caused by annealing.

Experimental Section

In our experiments, a mixture (1:1 in weight) of P3HT (M_w = 100 000 g mol^{-1}, M_w/M_n = 2.14, and regioregularity greater than 98.5% as determined by NMR, from Rieke Metals Inc.) and PCBM was dissolved in 1,2-dichlorobenzene (ODCB) and deposited by

[†] Laboratory of Materials and Interface Chemistry, Eindhoven University of Technology.
[‡] Dutch Polymer Institute, Eindhoven University of Technology.
[§] Fudan University.
[⊥] University of Duisburg-Essen.
* To whom correspondence should be addressed: e-mail j.loos@tue.nl; Ph +31-40-2473034.

10.1021/ma052590x CCC: $33.50
Published on Web 05/24/2006

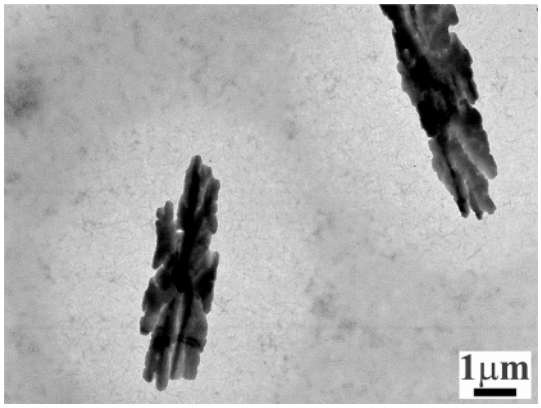

Figure 1. Bright-field transmission electron micrograph of P3HT/PCBM composite film upon thermal annealing.

spin-coating on glass substrates covered with 100 nm thick layers of indium tin oxide (ITO) and poly(ethylenedioxythiophene):poly(styrenesulfonate) (PEDOT:PSS) that form the electrode for hole collection. The composite P3HT/PCBM layer was ~70 nm thick. Afterward, thermal annealing was performed at 130 °C for 30 min. This temperature is below the apparent melting point ($T_m' \approx 215$ °C) of P3HT as determined by DSC.[25]

For transmission electron microscopy (TEM) investigation thin composite films were floated off from their substrates onto the surface of demineralized water and transferred to 400 mesh TEM grids. Subsequently, bright-field TEM morphology observation was conducted on a JEOL JEM-2000FX TEM operated at 80 kV.

Similarly treated samples but transferred on a glass slide were used for scanning near-field optical microscopy (SNOM). Measurements were performed in transmission mode using the SNOM head with a single-mode optical fiber coated with aluminum (both from NT-MDT, Moscow, Russia). The probes with tip aperture of 100 nm were prepared by chemical etching and have a transmission efficiency of $10^{-3}-10^{-4}$ and maximum output power of 5 μW. Two lasers, He−Ne ($\lambda = 632.8$ nm) and Nd:YAG ($\lambda = 532$ nm), were employed as radiation sources. The transmitted light was collected with a 20× objective and detected with a photomultiplier tube (PMT). For each line scan 256 data points were taken with a line scan frequency of 0.8−1.0 Hz.

Raman spectra were collected with a scanning Raman microscope "NANOFINDER" (NT-MDT, Moscow, Russia and Tokyo Instruments, Japan) in backscattering geometry. In all cases, the laser beam was focused down with a 100×/0.95 objective (Olympus, IX-70) in the inverted optical microscope. A confocal aperture of 60 μm diameter was used. The spatial lateral resolution of about 400 nm was estimated from independent measurements of Si/SiO_2 calibration grating. A Peltier-cooled CCD detector (Andor Technologies, Ireland) with 1024 × 256 pixels was operated at −55 °C. The acquisition time was fixed at 2 s for Raman mapping and 30 s for single spectra measurements.

The SNOM head was fixed on the piezo-XY stage of the Olympus inverted optical microscope which is a part of "Nanofinder". It is controlled by the same electronics and software as the Raman microscope. The SNOM and micro-Raman measurements can thus be performed with the same equipment and sample configuration.

Ultraviolet−visible (UV−vis) absorption spectra were recorded against glass (instead of air) on a Perkin-Elmer Lambda 900 UV−vis−NIR spectrometer.

Results and Discussion

Annealing at 130 °C for 30 min causes continuous crystallization and large-scale segregation of P3HT/PCBM composite films. Figure 1 shows a typical TEM image in bright-field contrast of the resulting morphology. The two dark areas represent large PCBM single crystals as can be seen from electron diffraction studies.[11,20] Upon thermal treatment, PCBM diffuses

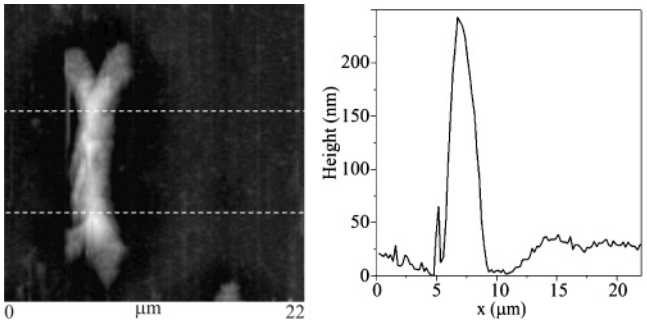

Figure 2. Topography image (left) and average profile of selected area (right) obtained from SNOM measurements.

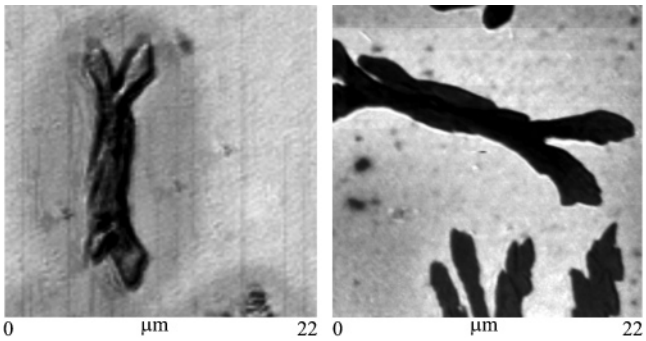

Figure 3. Optical contrast images obtained in SNOM transmission mode using monochromatic laser radiation with 632.8 nm (left) and 532 nm (right) wavelengths.

and aggregates into the crystals with lateral size in order of several micrometers. The PCBM crystals are surrounded by an area, which appears brighter in the image. On the basis of our knowledge related to annealing studies performed on the system MDMO-PPV/PCBM, we speculate that these areas are depleted from PCBM,[9,10,26] which would be a strong indication for high diffusive mobility of PCBM upon annealing, even when the annealing temperature is much below the melting temperature of the surrounding crystalline P3HT material. A better understanding of such diffusion features of PCBM is required to control phase segregation toward the desired morphology, which ultimately offers good device performance. Thus, in the following we like to demonstrate that the combined application of SNOM and Raman microscopy is able to provide new insights related to such features.

In a near-field optical measurement a single-mode optical fiber with a hole of around 100 nm in diameter on the sharp end is placed into the near field (distance of 2−4 nm) of the investigated sample. A near-field probe generates an evanescent field, the wavelength of which is shorter than that of the propagating field, and thus, a diffraction limit of around one-half of the wavelength of source light is circumvented.[27] The spatial resolution is then defined by the diameter of the hole. High-quality optical contrast images were obtained by this technique. It is especially important for analysis of materials on nanometer scale. A recent SNOM study on MEH-PPV/PCBM systems can be found in ref 28.

Near-field microscopic measurements provide a range of information about the P3HT/PCBM film studied. In Figure 2 a topography contrast image and the corresponding cross-sectional plot are shown. Different gray levels are consistent with the height of the features as can be seen from the corresponding cross-sectional plot. Three different regions can be distinguished in the sample: (a) a bright crystalline feature sticking out of the film plane and having a size of about 20 μm in length and 5 μm in width and a typical height of about 200 nm; (b) a dark

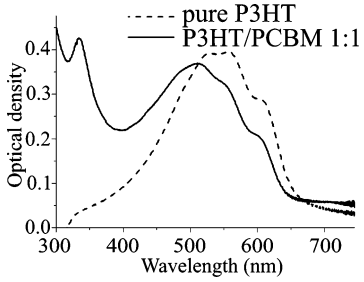

Figure 4. UV−vis absorption spectra of pure P3HT and its 1:1 by weight mixture with PCBM in the visible region.

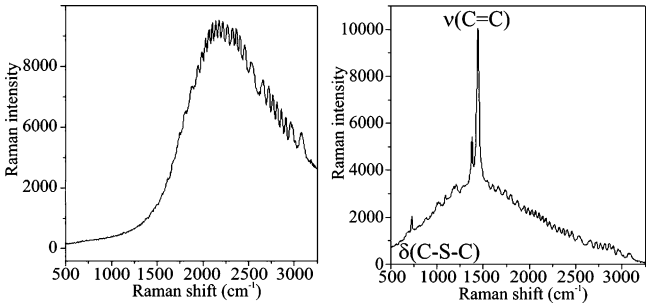

Figure 5. Fluorescence spectrum of PCBM (left) and Raman spectrum of P3HT (right).

zone surrounding this crystal, and (c) the remaining area representing the initial film plane. From the cross-sectional plot, we see that the zone surrounding the crystal is substantially deeper when compared with the initial film plane having a depth on the order of 30−50 nm, which is a first indication for depletion of PCBM similar to the system MDMO-PPV/PCBM.[9]

Optical contrast SNOM images taken in transmission mode are shown in Figure 3. The images are acquired at two different radiation wavelengths and show different contrast behavior. For our experimental setup, simultaneously topography and light absorbance measurements with a He−Ne laser of $\lambda = 632.8$ nm wavelength could be performed. Figure 3a shows the optical absorbance image of the same area as Figure 2a. For irradiation with such laser light the area with smaller thickness surrounding the crystal demonstrates a higher absorbance value compared to that of the initial film. However, at wavelength of 532 nm the absorbance behavior inverts: the absorbance of the initial film exceeds the absorbance of the crystal-close region. The crystals themselves have comparable transmission at both the 632.8 and 532 nm wavelengths. Unfortunately, our experimental setup does not allow simple change of the laser source so that we were not able to perform the optical absorbance measurement on the same sample area.

These differences in optical absorbance can be explained by monitoring the absorbance spectra of pure P3HT and a 1:1 by weight P3HT/PCBM mixture obtained using a conventional UV−vis spectrometer (Figure 4). After mixing the P3HT with PCBM the absorbance maximum in the visible spectrum has shifted from 570 nm to shorter wavelengths. Assuming that the areas surrounding the PCBM crystals are depleted of PCBM, the different absorption characteristics in dependence with the irradiation wavelength used can be explained. For both wavelengths, maximum absorption is found for the pure PCBM crystals, which mainly is related to their large thickness of several hundreds of nanometers. Comparing the initial film area, still composed 1:1 of P3HT/PCBM, with the area probably depleted by PCBM, the relative higher absorbance of 632.8 nm irradiation of the latter is related to the dominantly larger absorption of pure P3HT for such wavelength. In contrast, the slight higher absorbance of the initial film for 532 nm irradiation is caused by the somewhat similar absorbance characteristics of pure P3HT and the P3HT/PCBM mixture for such wavelength; however, the depletion zone is thinner and thus results in less total absorption.

Unfortunately, no Raman spectrum can be detected in such SNOM configuration because of extreme weak Raman signal ($I_{\text{Rayleigh}}/I_{\text{Raman}} \sim 10^6$) as well as of low transmission coefficient of the optical fiber used ($\sim 10^{-4}$) and limited applicable laser power. Thus, no information about chemical composition of the sample and distribution of components therein is available only from near-field optical microscopy. However, by using the equipment described above, near-field and Raman microscopy studies can be combined to obtain as much information as possible from the investigated sample.

Confocal Raman microscopic measurements were performed to get insight into the components distribution within the sampled film. First, the spectra of PCBM and P3HT as bulky pure materials were collected and are shown in Figure 5. A strong photoluminescence signal was detected from the pure PCBM (Figure 5, left) which has overlapped weak Raman bands. However, longer acquisition times and higher excitation power could not be used because of the reason of sample destruction. In the spectrum of P3HT (Figure 5, right) intensive Raman bands at 1442 and 1380 cm^{-1} can be attributed to C=C stretching vibrations of the thiophene ring and C−C skeletal stretching, respectively.[29] The Raman band at 728 cm^{-1} is assigned to the deformation vibration of the C−S−C bond. Significant fluorescent background is observed in the spectrum of P3HT as well.

Confocal Raman mapping was performed by monitoring the integrated intensity (Raman band area) of the ν(C=C) band at 1442 cm^{-1} at every point of the 225 μm^2 sample area with a

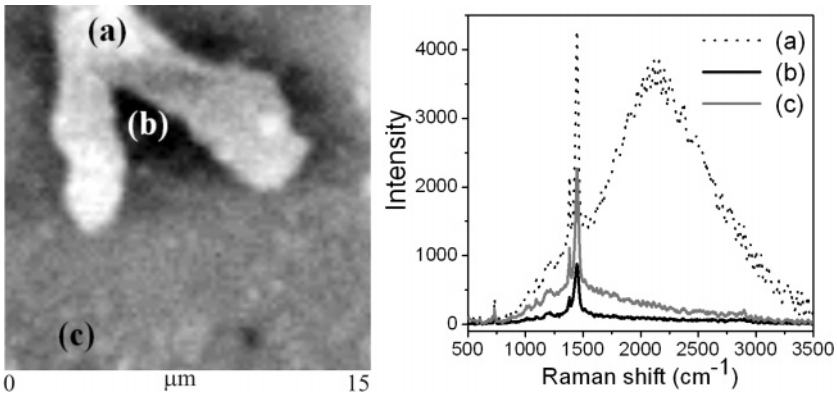

Figure 6. (a) Raman intensity distribution of the ν(C=C) band at 1450 cm^{-1} and (b) normalized spectra at positions (a)−(c) in part a.

step width between two consecutive measurement points of 150 nm. The 2D distribution of the sampled intensity is demonstrated in Figure 6. Since the height profile of the sample is known from the near-field optical measurements, the Raman image reflects obviously the thickness of the investigated film: high intensities at thick areas and low intensities at thin areas. To obtain the realistic information about the distribution of the components, Raman spectra were measured in three regions: (a) PCBM crystals, (b) area surrounding the crystals, and (c) the initial composite film area. The obtained spectra were normalized by averaged film thickness. The thickness of the initial film was estimated at 110 nm with roughness of 10 nm by independent AFM measurements. The height of crystals and thickness of, probably, PCBM depleted areas were evaluated from topography profiles obtained in SNOM experiments. The corresponding Raman spectra are also shown in Figure 6. The spectrum collected at point (a) has a strong fluorescent peak compared with spectra of the other areas, which is characteristic of bulk PCBM sample. Thus, the crystals contain predominantly PCBM material. However, Raman bands of P3HT with reasonable intensity also were found. Probably, the crystalline P3HT did not migrate from its initial position in the film sample to the other regions for annealing conditions as applied.

Raman modes of P3HT in the spectra of the crystal surrounding area and of the matrix demonstrate comparable intensity, indicating almost a similar amount of P3HT. The crystalline P3HT fibrils are not migrating; only PCBM depletes from the area surrounding the PCBM crystals so that the thin areas surrounding PCBM crystals still have the initial amount of P3HT in the composite film as-prepared. More detailed quantification of the local distribution of the amount of P3HT and PCBM is not possible by means of confocal Raman spectroscopy because of lack of lateral resolution and a heterogeneous sample thickness.

Conclusions

We have demonstrated that SNOM using irradiation sources with different wavelengths in the range of visible light is a suitable tool to gain insights in the component distribution of bulk heterojunction composite films based on P3HT and PCBM. After annealing the samples, phase segregation and continued crystallization are observed in topography images. Because the absorption characteristics of the components and their mixtures are different for the wavelengths used, relations between the local absorption characteristic of the sample and its organization can be resolved. From these data, it is assumed that large PCBM crystals are surrounded by a PCBM depleted area, still embedded in areas of the original film.

To further strengthen this statement, confocal Raman microscopy has been performed on bulk as well as on thin composite film samples. Also, Raman data suggest large-scale segregation and crystallization of PCBM upon annealing, which results in PCBM depletion areas. Moreover, from the presence of characteristic bands of P3HT at the position of the PCBM crystals, it can be concluded that the PCBM crystals are covered by P3HT fibrils. Further, the intensity of typical P3HT Raman bands in PCBM depletion areas as well as in the initial composite film is almost identical, which confirms that a similar amount of P3HT is present. In contrast to PCBM, P3HT stays at its initial location during the annealing treatment.

The results obtained help to better understand diffusion issues related to annealing procedures of bulk heterojunction polymer solar cells in general and in particular of the P3HT/PCBM composite, which is currently one of the most promising systems for polymer solar cells. Already for other systems based on PCBM[9,10,26] we could demonstrate that PCBM is very mobile, even for low annealing temperature far below 100 °C.[9] Finally, systematic time- and temperature-dependent studies monitoring the segregation in P3HT/PCBM composite films upon annealing are currently in progress.

Acknowledgment. This work is partly supported by the Dutch Polymer Institute (projects DPI #326 and #508). Further, we thank Senter/Novem for financial support. W.L. thanks European Union for financial support through European Union (EU) Asia-Link program ASI/B7-301/98/679-32.

References and Notes

(1) Brabec, C. J.; Sariciftci, N. S.; Hummelen, J. C. *Adv. Funct. Mater.* **2001**, *11*, 15.
(2) Bube, R. H. *Photoelectronic Properties of Semiconductors*; Cambridge University Press: Cambridge, 1992.
(3) Pope, M.; Swenberg, C. E. *Electronic Processes in Organic Crystals and Polymers*; Oxford University Press: Oxford, 1999.
(4) Yu, G.; Gao, J.; Hummelen, J. C.; Wudl, F.; Heeger, A. J. *Science* **1995**, *270*, 1789.
(5) Halls, J. J. M.; Walsh, C. A.; Greenham, N. C.; Marseglia, E. A.; Friend, R. H.; Moratti, S. C.; Holmes, A. B. *Nature (London)* **1995**, *376*, 498.
(6) Sariciftci, N. S.; Smilowitz, L.; Heeger, A. J.; Wudl, F. *Science* **1992**, *258*, 1474.
(7) Shaheen, S. E.; Brabec, C. J.; Sariciftci, N. S.; Padinger, F.; Fromherz, T.; Hummelen, J. C. *Appl. Phys. Lett.* **2001**, *78*, 841.
(8) van Duren, J. K. J.; Yang, X. N.; Loos, J.; Bulle-Lieuwma, C. W. T.; Sieval, A. B.; Hummelen, J. C.; Janssen, R. A. J. *Adv. Funct. Mater.* **2004**, *14*, 425.
(9) Yang, X. N.; van Duren, J. K. J.; Janssen, R. A. J.; Michels, M. A. J.; Loos, J. *Macromolecules* **2004**, *37*, 2151.
(10) Yang, X. N.; Alexeev, A.; Michels, M. A. J.; Loos, J. *Macromolecules* **2005**, *38*, 4289.
(11) Hoppe, H.; Drees, M.; Schwinger, W.; Schäffler, F.; Sariciftci, N. S. *Synth. Met.* **2005**, *152*, 117.
(12) Schilinsky, P.; Waldauf, C.; Brabec, C. J. *Appl. Phys. Lett.* **2002**, *81*, 3885.
(13) Padinger, F.; Rittberger, R. S.; Sariciftci, N. S. *Adv. Funct. Mater.* **2003**, *13*, 85.
(14) Brabec, C. J. *Solar Energy Mater. Solar Cells* **2004**, *83*, 273.
(15) Prosa, T. J.; Winokur, M. J.; Moulton, J.; Smith, P.; Heeger, A. J. *Macromolecules* **1992**, *25*, 4364.
(16) Bao, Z.; Dodabalapur, A.; Lovinger, A. *Appl. Phys. Lett.* **1996**, *69*, 4108.
(17) Sirringhaus, H.; Brown, P. J.; Friend, R. H.; Nielsen, M. M.; Bechgaard, K.; Langeveld-Voss, B. M. W.; Spiering, A. J. H.; Janssen, R. A. J.; Meijer, E. W. Herwig, P.; de Leeuw, D. M. *Nature (London)* **1999**, *401*, 685.
(18) Sirringhaus, H.; Tessler, N.; Friend, R. H. *Science* **1998**, *280*, 1741.
(19) Mihailetchi, V. D.; van Duren, J. K. J.; Blom, P. W. M.; Hummelen, J. C.; Janssen, R. A. J.; Kroon, J. M.; Rispens, M. T.; Verhees, W. J. H.; Wienk, M. M. *Adv. Funct. Mater.* **2003**, *13*, 43.
(20) Yang, X. N.; van Duren, J. K. J.; Rispens, M. T.; Hummelen, J. C.; Janssen, R. A. J.; Michels, M. A. J.; Loos, J. *Adv. Mater.* **2004**, *16*, 802.
(21) Camaioni, N.; Ridolfi, G.; Casalbore-Miceli, G.; Possamai, G.; Maggini, M. *Adv. Mater.* **2002**, *14*, 1735.
(22) Chirvase, D.; Parisi, J.; Hummelen, J. C.; Dyakonov, V. *Nanotechnology* **2004**, *15*, 1317.
(23) Yang, X. N.; Loos, J.; Veenstra, S. C.; Verhees, W. J. H.; Wienk, M. M.; Kroon, J. M.; Michels, M. A. J.; Janssen, R. A. J. *Nano Lett.* **2005**, 5, 579.
(24) Drees, M.; Hoppe, H.; Winder, C.; Neugebauer, H.; Sariciftci, N. S.; Schwinger, W.; Schäffler, F.; Topf, C.; Scharber, M. C.; Zhu, Z.; Gaudiana, R. *J. Mater. Chem.* **2005**, *15*, 5158.
(25) Malik, S.; Nandi, A. K. *J. Polym. Sci., Part B: Polym. Phys.* **2002**, *40*, 2073.
(26) Zhong, H. F.; Yang, X. N.; de With, B.; Loos, J. *Macromolecules* **2006**, *39*, 218.
(27) Kawata, S.; Inouye, Y. Near-field Optical Microscopy. In *Handbook of Vibrational Spectroscopy*; Chalmers, J., Griffiths, P., Eds.; Wiley-VCH: Chichester, 2002; Vol. 1, p 1460.
(28) McNeill, C. R.; Frohne, H.; Holdsworth, J. L.; Frust, J. E.; King, B. V.; Dastoor, P. C. *Nano Lett.* **2004**, *i*, 219.
(29) Baibarac, M.; Lapkowski, M.; Pron, A.; Lefrant, S.; Baltog, I. *J. Raman Spectrosc.* **1998**, *29*, 825.

MA052590X